CIRP Annals - Manufacturing Technology 72 (2023) 325–328

Contents lists available at ScienceDirect

CIRP Annals - Manufacturing Technology

journal homepage: https://www.editorialmanager.com/CIRP/default.aspx

Intelligent feedrate optimization using a physics-based and data-driven digital twin

Heejin Kim, Chinedum E. Okwudire (2)*

Smart and Sustainable Automation Research Laboratory, University of Michigan, Ann Arbor, USA

ARTICLE INFO

Article history:
Available online 29 April 2023

Keywords:
Computer numerical control (CNC)
Digital twin
Feedrate optimization

ABSTRACT

Intelligent manufacturing machines envisioned for the future must be able to autonomously select process parameters that maximize their speed while adhering to quality specifications. Accordingly, this paper proposes a framework and methodology for using a physics-based and data-driven digital twin of a feed drive to maximize feedrate while respecting kinematic and contour error limits. To correct for inaccuracies introduced by unmodeled dynamics and disturbances, the data-driven model is updated on-the-fly using sensor feedback. Experiments on a 3-axis CNC machine tool prototype are used to demonstrate up to 35% cycle time reduction without violating error tolerances compared to the status quo.

1. Introduction

Quality and productivity are two important and often competing attributes in manufacturing. Therefore, manufacturers often seek to maximize productivity subject to quality (tolerance) constraints. In practice, this goal is often achieved by trial-and-error. However, there is a push for self-optimizing (intelligent) manufacturing machines that are capable of, among other things, optimizing their speed while maintaining desired quality levels autonomously, without need for trial-and-error [1].

One major source of quality degradation in CNC machine tools is motion-induced servo error, which can result from the limited bandwidth of feedback controllers, flexible structures, nonlinear friction and backlash. Another source of servo error is cutting force. Since motion- and cutting-force-induced servo errors typically increase with speed, it is of interest to maximize motion speed subject to constraints on servo error.

The goal to maximize feedrate subject to motion and cutting force related constraints has been researched extensively under the topic of feedrate scheduling and feedrate optimization. Feedrate scheduling methods for CNC machines typically focus on maximizing feedrate in each NC block while keeping cutting force under desired levels via mechanistic force models [2]. On the other hand, the vast majority of feedrate optimization methods maximize feedrate subject to kinematic limits, like speed, acceleration, and jerk [3–5], where one of the ways to define maximum speed is using allowable cutting force [6]. However, the works in [2–6] do not directly restrict servo error.

To directly constrain servo error, some feedrate scheduling techniques maximize feedrate while regulating machining error due to tool deflection [7] or force-induced servo error [8,9] under desired tolerance. However, the works in [7–9] do not incorporate motion-induced servo error, which is important in toolpaths with high curvatures that can trigger significant structural vibration. Some feedrate optimization techniques impose kinematic limits, along with motion-induced servo error constraints via steady-state [10] or static (i.e., algebraic instead of using differential-equation) [11,12] servo models associated with motion velocity and acceleration. Still, their inability to incorporate dynamic components of servo error (e.g., dynamic servo error pre-compensation) limit their accuracy and ability to effectively optimize feedrate. A few works in feedrate optimization [13] constrain kinematics and motion-induced error via linear physics-based models of servo dynamics. However, the methods in [10–13] do not incorporate errors induced by cutting force. Moreover, all works in [7–13] cannot accurately constrain actual servo error when unmodeled dynamics or uncertainties exist in motion dynamics or cutting force. Hence, their efficacy to maximize feedrate with servo error constraints is very limited.

There is increasing interest in the utilization of digital twins (DTs) in manufacturing. A DT is a virtual representation, parallel to a physical system, built on a bi-directional link between simulation and actual data collection [1]. DTs incorporating physics-based models and measured data can provide more-accurate predictions of servo error for feedrate optimization [14,15]. For instance, a hybrid servo model, consisting of physics-based and data-driven models, was used in [15] to more-accurately predict the servo errors of a feed drive with unmodeled nonlinearities. However, no feedrate optimization was incorporated into the hybrid model. To address this shortcoming, this paper proposes an intelligent method to optimize feedrate with servo error constraints using a DT by making the following original contributions:

1) It augments the data-driven component of the hybrid model in [15] with a feature vector filtered by a periodic internal model to effectively predict servo errors due to motion and cutting forces on-the-fly.

* Corresponding author.
E-mail address: okwudire@umich.edu (C.E. Okwudire (2)).

https://doi.org/10.1016/j.cirp.2023.04.063
0007-8506/

2) It formulates an intelligent feedrate optimization approach capable of employing the developed DT to accurately impose servo error and kinematic limits in response to real-time data measured from a machine.

The outline of the paper is as follows: Section 2 presents the proposed intelligent framework exploiting DT composed of physics-based and data-driven servo models. The efficacy of the proposed approach is numerically and experimentally validated using a CNC machine tool prototype in Section 3. Section 4 concludes the paper and discusses future work.

2. Proposed intelligent feedrate optimization framework and approach

2.1. Framework for intelligent feedrate optimization

The framework for the proposed intelligent feedrate optimization is depicted in Fig. 1. First, an operator submits a part together with the desired contour error tolerance to an intelligent manufacturing machine. The goal of the machine is to autonomously produce the part as quickly as possible while respecting the given error tolerance and other machine constraints. The machine is equipped with a DT comprising a physics-based model of its servo dynamics together with a data-driven model that is trained on data gathered from the machine's sensors. The intelligent feedrate optimization algorithm uses the servo error predictions from the DT to determine the fastest feedrate to run the machine while respecting the acceptable limits for the servo errors (and the kinematic limits of the machine). The measured sensor output is compared with the predicted output and used to adjust the data-driven model and optimization algorithm in the next iteration of the feedrate optimization.

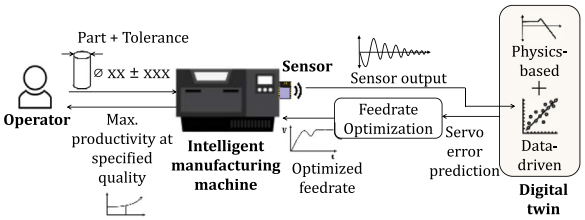

Fig. 1. Diagram of intelligent feedrate optimization framework using a DT.

2.2. DT-based servo error prediction including cutting force effects

A flowchart of the proposed intelligent feedrate optimization is given in Fig. 2 for the x-axis of a machine tool. Small batches (windows) $\boldsymbol{x}^j{}_d$ of a desired position trajectory are fed into an intelligent feedrate optimizer to produce the optimized motion command, $\boldsymbol{x}^j{}_c$ where j = 0, 1, 2, …, represents the batch index. The optimized motion commands are sent to the servo system $\boldsymbol{H}_x$ to produce actual position $\boldsymbol{x}^j$. The servo system is composed of a servo error pre-compensation $\boldsymbol{C}_x$ followed by machine dynamics $\boldsymbol{G}_x$, i.e., $\boldsymbol{H}_x = \boldsymbol{G}_x\boldsymbol{C}_x$.

A key requirement for the feedrate optimization is accurate prediction of servo errors which is achieved using a DT based on the hybrid model presented in [15] augmented with a periodic internal model to facilitate prediction of cutting-force-induced servo errors. The hybrid model takes input $\boldsymbol{x}^j{}_c$ and predicts the actual position $\hat{\boldsymbol{x}}^j$ using a physics-based model $\hat{\boldsymbol{H}}_{\boldsymbol{x}}$ of $\boldsymbol{H}_x$. The predictions $\hat{\boldsymbol{x}}^j$ do not capture the effects of unmodeled dynamics and cutting force disturbances. Therefore, the

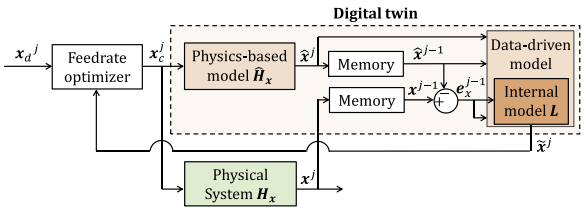

Fig. 2. Flowchart of intelligent feedrate optimization using digital twin (y-axis omitted for simplicity).

prediction error (delayed by one batch) is computed as $\boldsymbol{e}_x{}^{j-1}=\boldsymbol{x}^{j-1}-\hat{\boldsymbol{x}}^{j-1}$ and combined with $\hat{\boldsymbol{x}}^j$ and $\hat{\boldsymbol{x}}^{j-1}$ then fed into a data driven model to generate an improved prediction $\sim\boldsymbol{x}^j$ which is used for constraining servo errors in the feedrate optimization.

Each element $\sim x(t)$ of $\sim\boldsymbol{x}^j$ (where t = 0, T_s, $2T_s$, $3T_s$, … represents discrete time at sampling interval T_s) is computed as

$$\tilde{x}(t) = \boldsymbol{\psi}_t \boldsymbol{W} \tag{1}$$

where $\boldsymbol{\psi}_t$ is a row feature vector at time t and $\boldsymbol{W}$ is the corresponding column weight vector. The sub elements of $\boldsymbol{\psi}_t$ are given by

$$\boldsymbol{\psi}_t = \Big[\underbrace{1}_{:=\boldsymbol{\psi}_{t1}} \underbrace{\hat{x}(t-n_2T_s)\cdots\hat{x}(t)}_{:=\boldsymbol{\psi}_{t2}} \underbrace{e_x(t-n_3T_s)\cdots e_x(t-T_s)}_{:=\boldsymbol{\psi}_{t3}} \underbrace{\tilde{e}_x(t-n_3T_s)\cdots\tilde{e}_x(t-T_s)}_{:=\boldsymbol{\psi}_{t4}}\Big] \tag{2}$$

The first three elements $\boldsymbol{\psi}_{t1}$, $\boldsymbol{\psi}_{t2}$ and $\boldsymbol{\psi}_{t3}$ were contained in the hybrid model of [15]. They respectively represent a bias term, the past n_2 and current time steps of $\hat{x}$, and the past n_3 time steps of $\boldsymbol{e}_x$, where n_2 and n_3 are user defined. The fourth element $\boldsymbol{\psi}_{t4}$ is new in the proposed hybrid model. It consists of $\boldsymbol{\psi}_{t3}$ filtered by an internal model $\boldsymbol{L}$ that contains information about dominant frequency components of the cutting force. Specifically, the internal model, in Laplace domain, is a filter of the form

$$L(s) = \sum_i \frac{\omega_i^2}{s^2+\omega_i^2} \tag{3}$$

where s is the Laplace operator and ω_i (rad/s) are key harmonic frequencies contained in the cutting forces. Notice that the filter in Eq. (3) introduces infinite gain (poles) at each ω_i, hence ensuring that the data-driven model emphasizes dynamics occurring at ω_i.

$\sim\boldsymbol{x}^j$ at the j-th batch is predicted based on weight $\boldsymbol{W}$ from the previous batch $j-1$, which is trained as follows. Given that the length of each batch is n_w, for the 0-th batch, i.e., t = 0, T_s, …, $(n_w-1)T_s$, the weight vector $\boldsymbol{W}$ and its covariance matrix $\boldsymbol{P}$ are initialized using ridge regression with regularization factor λ

$$\boldsymbol{W} = \left(\lambda\boldsymbol{I}+\boldsymbol{\psi}_t^{\mathrm{T}}\boldsymbol{\psi}_t\right)^{-1}\boldsymbol{\psi}_t^{\mathrm{T}}x(t) \tag{4}$$

$$\boldsymbol{P} = \left(\lambda\boldsymbol{I}+\boldsymbol{\psi}_t^{\mathrm{T}}\boldsymbol{\psi}_t\right)^{-1}$$

For the rest of batches j = 1, 2, …, i.e., $t = n_wT_s$, $(n_w+1)T_s$, …, $\boldsymbol{W}$ and $\boldsymbol{P}$ are corrected via recursive least-squares using a forgetting factor f_0 as

$$\boldsymbol{W} \leftarrow \boldsymbol{W}+\boldsymbol{k}(x(t)-\boldsymbol{\psi}_t\boldsymbol{W}),\ \text{where}\ \boldsymbol{k} = \boldsymbol{P}\boldsymbol{\psi}_t^{\mathrm{T}}\left(f_0+\boldsymbol{\psi}_t\boldsymbol{P}\boldsymbol{\psi}_t^{\mathrm{T}}\right)^{-1} \tag{5}$$

$$\boldsymbol{P} \leftarrow (\boldsymbol{P}-\boldsymbol{k}\boldsymbol{\psi}_t\boldsymbol{P})/f_0$$

Using the final weight in batch $j-1$ to substitute $\boldsymbol{W}$ in Eq. (1), $\sim\boldsymbol{x}^j$ can be predicted using the feature vector $\boldsymbol{\psi}_t$ formulated by Eq. (2). Since the past sensor data $\boldsymbol{x}^{j-1}$ is provided up to $t = (jn_w-1)T_s$, for entries in batch j that have unavailable terms in $\boldsymbol{\psi}_{t3}$, $\boldsymbol{e}_x$ is approximated using predicted values $\sim\boldsymbol{x}$, i.e.,

$$\boldsymbol{e}_x = \boldsymbol{x}-\hat{\boldsymbol{x}} \approx \sim\boldsymbol{x}-\hat{\boldsymbol{x}} \tag{6}$$

and $\boldsymbol{\psi}_{t4}$ can be similarly expressed using the approximated $\boldsymbol{\psi}_{t3}$.

Finally, we show that $\sim x(t)$ is linear in terms of $\boldsymbol{x}^j{}_d$, by showing that the only alterable feature in $\boldsymbol{\psi}_t$, which is the last term in $\boldsymbol{\psi}_{t2}$ (i.e., $\hat{x}(t)$), is linear in $\boldsymbol{x}^j{}_d$. Let $\boldsymbol{\Phi}_x \in \mathbb{R}^{n_h\times n_h}$ be the matrix (lifted domain) representation of $\hat{\boldsymbol{H}}_{\boldsymbol{x}}$ truncated by length n_h. The last n_w rows in $\boldsymbol{\Phi}_x$ can further be decomposed into two parts: its first n_h-n_w columns $\boldsymbol{\Phi}_{x,p}$ and its last n_w columns $\boldsymbol{\Phi}_{x,c}$ as

$$\Phi_x = \begin{bmatrix} \vdots & \vdots \\ \Phi_{x,p} & \Phi_{x,c} \end{bmatrix} \tag{7}$$

If $\boldsymbol{x}_{cp}$ represents the last n_h-n_w elements of the $\boldsymbol{x}_c$ at past timesteps, $\hat{x}(t)$ can be re-written as

$$\boldsymbol{x}\,j = \Phi_{x,c}\boldsymbol{x}_d^j + \Phi_{x,p}\boldsymbol{x}_{cp} \tag{8}$$

$$\therefore\hat{x}(t) = \boldsymbol{M}_t\Phi_{x,c}\boldsymbol{x}_d^j + \boldsymbol{M}_t\Phi_{x,p}\boldsymbol{x}_{cp}$$

where $\boldsymbol{M}_t$ is a selection matrix that picks the entry at timestep t.

Let the alterable and unalterable features in Eq. (2) be ψ_{ta} (= $\hat{x}(t)$) and ψ_{tu}, and their corresponding sub-weights be $\boldsymbol{W}_a$ and $\boldsymbol{W}_u$ respectively. Then, using Eq. (8), $\sim x(t)$ is linearly related to $\boldsymbol{x}^j_d$ by

$$\sim x(t) = \boldsymbol{\psi}_{ta}\boldsymbol{W}_a + \boldsymbol{\psi}_{tu}\boldsymbol{W}_u \tag{9}$$

$$= \underbrace{\boldsymbol{M}_t\Phi_{x,c}\boldsymbol{W}_a}_{:=\boldsymbol{T}_{xt}\boldsymbol{x}^j_d} + \underbrace{\boldsymbol{M}_t\Phi_{x,p}\boldsymbol{x}_{cp}\boldsymbol{W}_a + \boldsymbol{\psi}_{tu}\boldsymbol{W}_u}_{:=T_{0t}}$$

2.3. Intelligent feedrate optimization using DT

The feedrate optimization using the DT is formulated in accordance with the authors' previous work [13]. Taking the x-axis, for example, a desired trajectory $X_d = f(p)$ is parametrized with respect to a normalized, monotonically increasing path variable $\boldsymbol{p}$. Then, $X_d(t)$ is linearized as $x_d(t)$ with respect to $p(t)$ using an estimated linearization point $p_e(t)$ as

$$x_d(t) = \left.\frac{\partial f}{\partial p}\right|_{p=p_e(t)} \cdot (p(t) - p_e(t)) + f(p_e(t)) \tag{10}$$

The procedure for computing the optimal $\boldsymbol{p}^j$ (corresponding to the optimal feedrate) using the DT is as follows. The path variable $\boldsymbol{p}^j$ is maximized under monotonicity, maximum feedrate, and axis-acceleration constraints as

$$\begin{aligned} &\max \mathbf{1}^{\mathrm{T}}\boldsymbol{p}^j \\ &\text{s.t. } p(t-1) \le p(t) \le 1 \\ &D\left[\boldsymbol{p}^j\right] \le \boldsymbol{V}_{max}T_s \\ &\left|D^2\left[\boldsymbol{x}^j_d\right]\right| \le \boldsymbol{A}_{max}T_s^2 \end{aligned} \tag{11}$$

where $\mathbf{1}$ is a ones-vector, D is a difference operator, and $\boldsymbol{V}_{\max}$ and $\boldsymbol{A}_{\max}$ are the vectorized representations of feedrate and acceleration limits, respectively. In addition, kinematic and dynamic continuity between adjacent windows is enforced. The process described above for the x-axis can be applied to the y-axis.

The position predictions $\sim\boldsymbol{x}^j$ of the DT are integrated into the feedrate optimization by using them to constrain the servo errors. To do this, we leverage the fact that the proposed hybrid model is a linear operator, because its physics-based and data-driven components are both linear operators. Therefore, the predicted servo error $\sim\varepsilon_x(t)$ for $t = jn_wT_s, \ldots, ((j+1)n_w-1)T_s$ in the j-th batch can be expressed using $\sim x(t)$ from Eq. (9) as

$$\sim\varepsilon_x(t) = x_d(t) - \sim x(t) = (\boldsymbol{M}_t - \boldsymbol{T}_{xt})\boldsymbol{x}^j_d - \boldsymbol{T}_{0t} \tag{12}$$

The processes described above are repeated for the y-axis to compute $\sim\varepsilon^j_y$. Finally, contour error ε can be estimated from DT-predicted axis tracking errors $\sim\varepsilon_x$ and $\sim\varepsilon_y$ and constrained under tolerance E_{max} using a linear approximation [16] as

$$|\boldsymbol{\varepsilon}| = \left|-\sin(\boldsymbol{\theta})\boldsymbol{\varepsilon}^{\sim}_x + \cos(\boldsymbol{\theta})\boldsymbol{\varepsilon}^{\sim}_y\right| \le \boldsymbol{E}_{max} \tag{13}$$

where $\boldsymbol{\theta}$ is inclination angle of the curve $(\boldsymbol{x}_d\boldsymbol{y}_d)$, and $\boldsymbol{E}_{max}$ is the vectorised representation of E_{max}.

Overall, the DT-based intelligent feedrate optimization becomes a linear programming in terms of the decision variable $\boldsymbol{p}^j$.

3. Validation

3.1. Numerical validation of DT-based servo error prediction

A simple simulation case study is presented here to highlight the importance of augmenting the hybrid model in [15] with an internal model to enable accurate prediction of motion-induced and cutting-force-induced servo errors. To do so, a desired trajectory on x-axis with its velocity shown in Fig. 3 is selected with maximum velocity as 100 mm/s and acceleration as 1 m/s^2. The simulated output $\boldsymbol{x}$ is modeled as sum of motion-induced position $\boldsymbol{x}_m$ and cutting-force-induced position $\boldsymbol{x}_f$ as

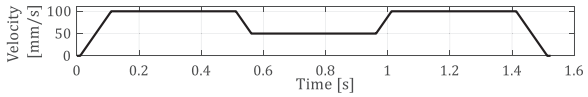

Fig. 3. Velocity of desired trajectory on x-axis.

$$\boldsymbol{x} = \boldsymbol{x}_m + \boldsymbol{x}_f = \boldsymbol{H}_x\boldsymbol{x}_d + \boldsymbol{x}_f \tag{14}$$

$$x_f(t) = 0.01\dot{x}_m(t)\sin(\omega_f t)$$

where ω_f = 523.6 rad/s (5000 rpm) is used. For the DT, n_w = 20, n_2 = 2, n_3 = 20, λ = 0.01 and f_0 = 1 are used; for the internal model, $\omega_i = \omega_f$ is used. The data-driven model is trained for one cycle of the trajectory in Fig. 3 prior to testing. The physics-based model $\widehat{\boldsymbol{H}}_x$ is defined as a 2nd order system with ω_n= 157 rad/s and ζ = 0.05; $\boldsymbol{H}_x$ is modeled with mismatch in coefficients by 10% deviation as ω'_n= 1.1·ω_n and ζ' = 0.9·ζ, i.e.,

$$\widehat{\boldsymbol{H}}_x = \left(2\zeta\omega_n s + \omega_n^2\right)/\left(s^2 + 2\zeta\omega_n s + \omega_n^2\right) \tag{15}$$

$$\boldsymbol{H}_x = \left(2\zeta^{\{\}'}\omega_n^{\{\}'}s + \omega_n^{\{\}'2}\right)/\left(s^2 + 2\zeta^{\{\}'}\omega_n^{\{\}'}s + \omega_n^{\{\}'2}\right)$$

Fig. 4 shows the prediction error using the DT without and with the internal model. Using the internal model, the RMS prediction error of $\boldsymbol{x}$ is reduced by 27.7%. The following Sections 3.2 and 3.3 will highlight the performance of the DT-based feedrate optimization using the internal model in experiments.

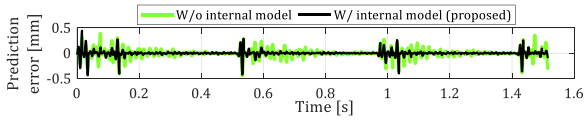

Fig. 4. Prediction error using DT without and with the internal model.

3.2. Experimental setup

For experimental validation, Nomad3 three-axis CNC machine tool prototype is used. The optimization algorithm is implemented on dSPACE 1007 real-time control board running at 500 Hz sampling rate, connected to DRV8825 stepper motor drivers for x, y, and z-axes stepper motors. Renishaw RKLC20-S optical linear encoders are attached on the x and y- axes gantries to measure x and y- axes positions that are fed back to dSPACE 1007.

A frequency response function (FRF) is measured for the x and y axis of the machine to identify the machine dynamic component of physics-based model, $\hat{\boldsymbol{G}}_x$ and $\hat{\boldsymbol{G}}_y$. The input of each FRF measurement is a swept sine acceleration command to the stepper motors, and the output is the relative acceleration between the x and y axis using two PCB 393B05 shear accelerometers. Then, the measured FRFs are modelled via curve fitting. The discrete-time transfer function of $\hat{\boldsymbol{G}}_x$ and $\hat{\boldsymbol{G}}_y$ with T_s = 2 ms are

$$\widehat{\boldsymbol{G}}_x = \frac{0.487z^3 - 0.8471z^2 + 0.7827z - 0.3768}{z^4 - 2.149z^3 + 2.037z^2 - 0.9917z + 0.1495} \tag{16}$$

$$\widehat{\boldsymbol{G}}_y = \frac{0.4378z^3 + 0.4994z^2 - 0.0569z + 0.0128}{z^4 - 0.1282z^3 + 0.0217z^2 - 0.001z + 0.0001}$$

The servo error pre-compensation $\boldsymbol{C}_x$ and $\boldsymbol{C}_y$ are formulated using $\hat{\boldsymbol{G}}_x$ and $\hat{\boldsymbol{G}}_y$ via limited-preview filtered B-spline method in [17].

3.3. Experimental validation of DT-based feedrate optimization

This section validates proposed DT-based approach by comparing its performance with physics-based approach (without data-driven model) and conservative method generated using a trapezoidal acceleration profile with kinematic limits tuned by trial-and-error to achieve the servo error tolerances. A butterfly toolpath [18] in Fig. 5 is used for air cutting and machining an aluminum workpiece with 3.175 mm diameter flat-end mill and spindle speed of 7000 rpm. Kinematic limits are set as V_{max} = 30 mm/s and A_{max} = 1 m/s^2 in the feedrate optimization; n_w = 30, n_2 = 2, n_3 = 30, λ = 0.01 and f_0 = 1 are used in the data-driven model, which is pre-trained using one cycle of physics-based feedrate

optimization. The frequencies ω_i of $\boldsymbol{L}$ in Eq. (3) are experimentally identified as in Fig. 6, based on encoder data measured during cutting. A safety factor of 25% is applied to the desired tolerance, i.e., a contour error bound of E_{max} = 0.12 mm is applied in optimization to achieve error tolerance of 0.15 mm in experiments.

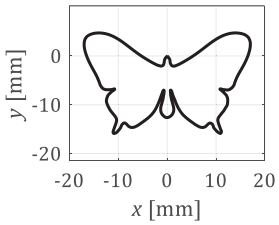

Fig. 5. Desired toolpath.

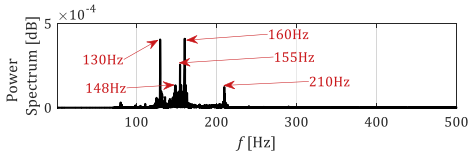

Fig. 6. Experimentally identified disturbance frequencies for internal model.

Figs. 7 and 8 show the profiles of commanded feedrate, acceleration, contour error, and prediction error of x and y using conservative, physics-based, and DT-based approaches in air-cutting and machining, respectively. The DT-based approach reduces the prediction error in x-axis by 47.3% and 45.7%, and in y-axis by 4.0% and 34.6% during air-cutting and machining, respectively, compared to the physics-based method, which allows the tolerance to be satisfied. However, the physics-based method violates the tolerance due to unmodeled dynamics and/or cutting force. As a result, the proposed approach completes the motion 35.0% and 17.2% faster than the conservative method in air-cutting and machining, respectively, without sacrificing contouring accuracy. The DT-based algorithm runs in real-time by computing the entire trajectory for machining within 2.04 s.

Fig. 9 shows the machined surfaces using trajectories from Fig. 8. The surface quality of the proposed approach is improved compared to that of physics-based approach, while staying similar to that of conservative part.

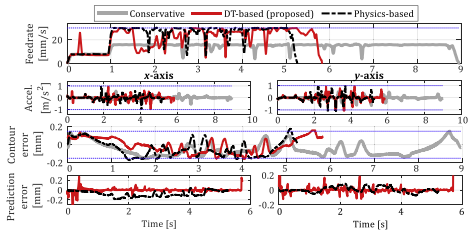

Fig. 7. Feedrate, acceleration, contour error and prediction error using conservative, physics-based and DT-based feedrate optimization in air-cutting.

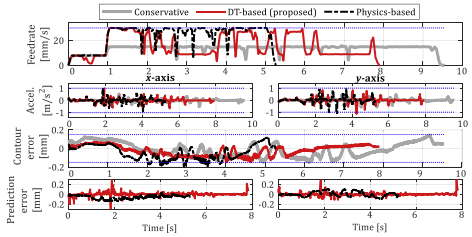

Fig. 8. Feedrate, acceleration, contour error and prediction error using conservative, physics-based and DT-based feedrate optimization in machining.

4. Conclusion and future work

This paper presents a framework and approach for intelligent feedrate optimization using a DT that allows for a machine to produce parts with desired part quality specifications as quickly as possible. The DT is first built on a physics-based dynamics model. Then, a data-driven model with an internal model is updated on-the-fly to adapt to unknown dynamics and cutting force disturbances. Using experiments on a CNC machine tool prototype, the proposed approach showed its performance in accurately constraining the contour error while reducing cycle time by up to 35% compared to conservative approach. The future work will explore improving robustness of the data-driven model, and machine-to-machine learning using the data-driven model in a DT framework.

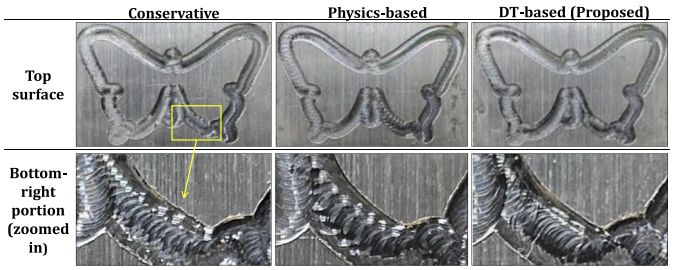

Fig. 9. Machined surfaces using the three approaches investigated.

Declaration of Competing Interest

The authors declare that they have no known competing financial interests or personal relationships that could have appeared to influence the work reported in this paper.

Acknowledgements

This work is partially funded by the National Science Foundation grant # 1931950. We thank Dr. Keivan Ahmadi for his feedback.

References

[1] Möhring HC, Wiederkehr P, Erkorkmaz K, Kakinuma Y (2020) Self-Optimizing Machining Systems. *CIRP Annals* 69(2):740–763.
[2] Erdim H, Lazoglu I, Ozturk B (2006) Feedrate Scheduling Strategies for Free-Form Surfaces. *International Journal of Machine Tools and Manufacture* 46(7–8):747–757.
[3] Altintas Y, Erkorkmaz K (2003) Feedrate Optimization for Spline Interpolation in High Speed Machine Tools. *CIRP Annals* 52(1):297–302.
[4] Erkorkmaz K, Chen QGC, Zhao MY, Beudaert X, Gao XS (2017) Linear Programming and Windowing Based Feedrate Optimization for Spline Toolpaths. *CIRP Annals* 66(1):393–396.
[5] Dong J, Ferreira PM, Stori JA (2007) Feed-Rate Optimization with Jerk Constraints for Generating Minimum-Time Trajectories. *International Journal of Machine Tools and Manufacture* 47(12–13):1941–1955.
[6] Erkorkmaz K, Layegh SE, Lazoglu I, Erdim H (2013) Feedrate Optimization for Freeform Milling Considering Constraints From the Feed Drive System and Process Mechanics. *CIRP Annals* 62(1):395–398.
[7] Fussell BK, Jerard RB, Hemmett JG (2001) Robust Feedrate Selection for 3-Axis NC Machining Using Discrete Models. *Journal of Manufacturing Science and Engineering* 123(2):214–224.
[8] Yang J, Aslan D, Altintas Y (2018) A Feedrate Scheduling Algorithm to Constrain Tool Tip Position and Tool Orientation Errors of Five-Axis CNC Machining Under Cutting Load Disturbances. *CIRP Journal of Manufacturing Science and Technology* 23:78–90.
[9] Altintas Y, Yang J, Kilic ZM (2019) Virtual Prediction And Constraint of Contour Errors Induced by Cutting Force Disturbances on Multi-Axis CNC Machine Tools. *CIRP Annals* 68(1):377–380.
[10] Chen M, Xu J, Sun Y (2017) Adaptive Feedrate Planning for Continuous Parametric Tool Path With Confined Contour Error and Axis Jerks. *The International Journal of Advanced Manufacturing Technology* 89(1):1113–1125.
[11] Dong J, Stori JA (2007) Optimal Feed-Rate Scheduling for High-Speed Contouring. *Journal of Manufacturing Science and Engineering* 129(1):63–76.
[12] Fan W, Gao XS, Lee CH, Zhang K, Zhang Q (2013) Time-Optimal Interpolation for Five-Axis CNC Machining Along Parametric Tool Path Based on Linear Programming. *The International Journal of Advanced Manufacturing Technology* 69(5):1373–1388.
[13] Kim H, Okwudire CE (2020) Simultaneous Servo Error Pre-Compensation and Feedrate Optimization with Tolerance Constraints Using Linear Programming. *The International Journal of Advanced Manufacturing Technology* 109(3):809–821.
[14] Chang YC, Chen CW, Tsao TC (2018) Near Time-Optimal Real-Time Path Following Under Error Tolerance and System Constraints. *Journal of Dynamic Systems, Measurement, and Control* 140(7):071004.
[15] Chou CH, Duan M, Okwudire CE (2021) A Linear Hybrid Model for Enhanced Servo Error Pre-Compensation of Feed Drives with Unmodeled Nonlinear Dynamics. *CIRP annals* 70(1):301–304.
[16] Koren Y, Lo CC (1991) Variable-Gain Cross-Coupling Controller for Contouring. *CIRP Annals* 40(1):371–374.
[17] Duan M, Yoon D, Okwudire CE (2018) A limited-Preview Filtered B-Spline Approach to Tracking Control–With Application to Vibration-Induced Error Compensation of a 3D Printer. *Mechatronics* 56:287–296.
[18] Yang S, Ghasemi AH, Lu X, Okwudire CE (2015) Pre-Compensation of Servo Contour Errors Using a Model Predictive Control Framework. *International Journal of Machine Tools and Manufacture* 98:50–60.